

Structural study of the rare earth compounds: $\text{Sm}(\text{OH})_3$, NdOHCO_3 , CeO_2 , and Ho_2O_3 , prepared by Chemical Bath Deposition, and its correlation with crystal growth mechanism


M. Chávez Portillo, M.A. Vicencio Garrido, Y. Ramos Reynoso, H. Juárez Santiesteban, A. Reyes Díaz, O. Portillo Moreno

We present the preliminary theoretical-experimental study of the structural properties for rare earths: hydroxide, hydroxycarbonate and Oxide; $\text{Sm}(\text{OH})_3$, NdOHCO_3 , CeO_2 , and Ho_2O_3 powders, respectively. In the experimental preparation, Chemical Bath Deposition (CBD) technique is applied at $\sim 20 \pm 2$ °C. In our experimental conditions, the parameters of crystal growth are: concentration of progenitor reagents, stirring, pH and temperature, remain constant. The chemical kinetics of crystal growth is systematically examined at key synthesis steps, considering the physicochemical and electrodynamic parameters: ionic radii, electron affinity, and hydration enthalpy of the rare earth (Sm^{3+} , Nd^{3+} , Ce^{3+} , and Ho^{3+}) cation. The main objective of this report is to investigate the theoretical-experimental correlation associated with the experimental conditions and the physicochemical parameters in the synthesis of hydroxide, hydrocarbonates and oxide. The crystallographic study of the powders is carried out using the X-ray Diffraction (XDR) technique. Analyzing the crystal phase, it is found that $\text{Sm}(\text{OH})_3$ and NdOHCO_3 present hexagonal crystal phase, CeO_2 and Ho_2O_3 are identified cubic crystal structure. The quantified grain size turns out to be: $\text{Sm}(\text{OH})_3$: $\sim 1.40 - 2.03$ nm, NdOHCO_3 : $\sim 14.33 - 22.25$ nm; CeO_2 : $\sim 1.65 - 3.05$ nm; and Ho_2O_3 : $\sim 3.72 - 6.08$ nm. The Dislocation density (δ) is: $\text{Sm}(\text{OH})_3$: $\sim 2.47 - 5.10 \times 10^{17}$ lines/m²; NdOHCO_3 : $2.01 - 4.68 \times 10^{15}$ lines/m²; CeO_2 : $1.07 - 3.67 \times 10^{17}$ lines/m².




Introduction

Single crystal hydroxide, hydrocarbonates and oxides containing rare earths (RE) present diverse morphology, chemical composition, structural and optical properties of interest to the scientific community [1]. The structural properties of inorganic RE nanocrystals are systematically examined by various research groups and theoretical-experimental studies have been carried out, since they show a significant optical-structural correlation [2]. It is of primary interest to investigate the structural properties of nanocrystals; these are significantly correlated with the optical response. Consequently, RE inorganic nanocrystals are strong candidates for their application as base material in the construction of optoelectronic devices, as well as in a variety of applications [3,4]. On the other hand, crystal growth is one interesting and vitally important feature science, which has contributed to significant improvements in producing nanocrystals with specific properties [5]. However, the synthesis conditions of crystal growth require systematic and optimal control of the physicochemical and thermodynamic parameters depending on the applied technique [6,7,8]. Some interesting reports of crystal growth are available investigating RE cations by systematic study and their experimental theoretical correlation with physicochemical parameters [9]. Furthermore, the inorganic nanocrystals of RE are systematically prepared, which allows monitoring the different parameters associated with crystal growth, with the aim of controlling the decrease in grain size (GS). Therefore, to reduce the relative cost between other parameters associated with the synthesis and the experimental equipment used, crystal growth parameters can be systematically controlled. A recently proposed mechanism of grain boundary migration known as the “mixed control mechanism” and the associated principles of microstructural evolution represent the basis of the solid-state single crystal growth technique [10]. Various ER synthesis techniques, both chemical and physical; have been reported in the last decades: hydrothermal synthesis [11],

spray pyrolysis technique [12], thermal decomposition [13], Chemical Bath Deposition (CBD) technique [7,8]. CBD technique has been applied in the preparation of various nanocrystals; Semiconductors [16], ER oxides [7,8,14,15]. In this paper we systematically apply the CBD technique for the synthesis in aqueous solution of four RE, and the crystal growth parameters constant throughout the chemical synthesis process. The inorganic nanocrystals examined here are: samarium hydroxide $\text{Sm}(\text{OH})_3$, neodymium hydrocarbonates (NdOHCO_3), cerium oxide (CeO_2), and holmium oxide (Ho_2O_3) were previously reported [7,8,14,17], now focuses on the study related to physicochemical parameters in chemical synthesis. Therefore, our study focuses specifically on the systematic structural analysis associated at crystalline parameters that govern the chemical kinetics performed. In particular, our study focuses specifically on

M. Chávez Portillo 

Universidad Politécnica de Puebla,
Cuanalá, Puebla, 72640, México.

M.A. Vicencio Garrido , Y. Ramos Reynoso ,
H. Juárez Santiesteban 

Centro de Investigación en Dispositivos Semiconductores,
Instituto de Ciencias, Universidad Autónoma de Puebla
Puebla, Puebla, 72592, México.

A. Reyes Díaz 

Universidad de Sonora
Hermosillo, Sonora, 83000, México.

O. Portillo Moreno 

Facultad de Ciencias Químicas
Benemérita Universidad Autónoma de Puebla
Puebla, Puebla, 72570, México.

Received: September 27th, 2022

Accepted: September 15th, 2023

Published: September 20th, 2023

© 2023 by the authors. Creative Commons Attribution
https://doi.org/10.47566/2023_syv36_1-230901

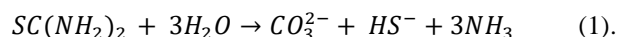
the systematic structural analysis associated with the crystalline parameters that govern the chemical kinetics performed in aqueous solution. In this report, we consider the creation of the coordination complex cation in the critical step of chemical synthesis. The creation of the corresponding coordination complex ion of chemical formula $[M(NH_3)_6]^{3+}$, (where $M = Sm^{3+}$, Nd^{3+} , Ce^{3+} , and Ho^{3+}), which is a key chemical parameter in the intermediate stage of chemical kinetics. The experimental characterization of the structural part is investigated by X-Ray Diffraction (XRD) technique. Taking XRD diffractograms, then using the Debye-Scherrer equation GS is quantified numerically. The morphology and optical properties have been previously published by some of us [7,8,14,17]. A systematic analysis of the products obtained is carried out and the comparative study in the key stages of crystal growth. The influence of the following physicochemical parameters: electronic affinity, ionic radii, are associated in the chemical kinetics of the crystalline growth.

Experimental

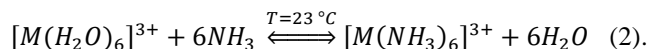
Chemical equilibria associated with crystal growth

$Sm(OH)_3$, $NdOHCO_3$, CeO_2 , and Ho_2O_3 inorganic nanocrystals, are systematically prepared applying the CBD technique [7,8,14,17]. It is important to point out that in the preparation of these nanocrystals, the parameters of crystalline growth are kept constant: pH, agitation, progenitor reagents, reaction time and temperature [18]. The chemical synthesis to prepare the inorganic nanocrystals, is shown in different stages proposed according to the following chemical balances:

Initially, the hydrolysis of thiourea dissociates in aqueous solution under RT conditions, generating HS^- y CO_3^{2-} ions, previously identified by the FTIR technique [7,8,14,17,19,20]



The kinetic equilibrium in the capture of L-NH₃ molecules called ligands (L), as well as the simultaneous release of H₂O molecules; according to the theory of coordination complexes, shows the following chemical equilibrium



The alkaline chemical synthesis medium (pH = 8.3-8.5) is achieved by mixing thiourea and potassium hydroxide (KOH), creating $M(OH)_{3(aq)}$ colloidal suspension. The systematic addition of the ammonium nitrate solution (NH_4NO_3) in the colloidal suspension, generates the color change of the mixture (depends on the type of cation M^{3+}).

Under optimal experimental conditions, the coordination complex $[M(NH_3)_6]^{3+}$ cation is generated indirectly and moderately [21]



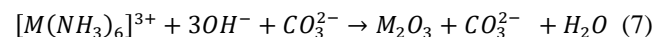
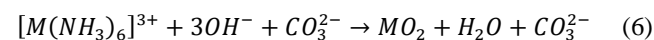
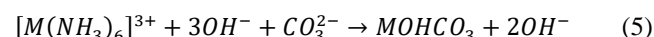
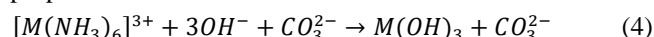
The relative thermodynamic stability of $[M(NH_3)_6]^{3+}$ cation, is governed by physicochemical properties (electron affinity, ionic radii, bond length, etc.) [22]. Additionally, also the coordination number and hydration enthalpy

Table 1. Hydration enthalpy (ΔH_{hyd}^0) for the Sm^{3+} , Nd^{3+} , Ce^{3+} , and Ho^{3+} cations.

Cation	ΔH_{hyd}^0 (kJ/mol)	
	Experimental	Calculations
Sm^{3+}	1509	1480
Nd^{3+}	3420	3460
Ce^{3+}	6300	6260
Ho^{3+}	3600	3640

(∇H_{hyd}^0), are parameters associated with chemical kinetics of crystal growth. The ∇H_{hyd}^0 of M^{3+} cation are compiled at Table 1. The semi empirical numerical values contemplated here, allow us to examine the correlation that exists at kinetics of crystal growth and the relative thermodynamic stability according to the equilibria presented at equations (2) and (3). The experimental control of the physicochemical parameters, ionic and molecular environment, relative stability of the M^{3+} cation (surrounded by six polar H₂O molecules) requires further study for crystal growth to be understood more clearly [23]. Commonly, the primary hydration sphere made up of H₂O (normally there are six), are chaotically oriented towards the M^{3+} cation. Most complexes with coordination number six have octahedral molecular symmetry. However, these geometries are not perfect octahedrons (six equal M-L distances and all angles are 90°) because they suffer from molecular distortion. Molecular distortion is a poorly studied geometric parameter and requires studies to be examined [24]. (ΔH_{hyd}^0 , is associated with the phenomenon of crystal growth in chemical thermodynamic processes. It is an intrinsic property in ionic compounds [25].

The key stage in crystal growth is based on the capture of OH^- and CO_3^{2-} ions and the simultaneous slow release of NH_3 molecules, the following chemical equilibria are proposed



Comparing the numerical data of ∇H_{hyd}^0 compiled at Table 1, a semiempirical increase in capture of H₂O molecules and the release of L-NH₃ molecules related to the relative thermodynamic stability according at following order: $Sm^{3+} < Nd^{3+} < Ho^{3+} < Ce^{3+}$. However, the increase shows some semi-empirical energetic correlation (except for the Ho^{3+} cation). On the other hand, electron affinity is the energy released by a neutral gaseous atom, semi-empirically associated with its fundamental energy level by capturing an electron from some other chemical species. According to the periodic Table of the elements, the electronic affinity increases by decreasing the size of the atom, it increases from left to right and from the bottom to the top, with similar behavior in electronegativity. Table 2 shows the electron affinity and ionic radii of the cations examined here [26,27].

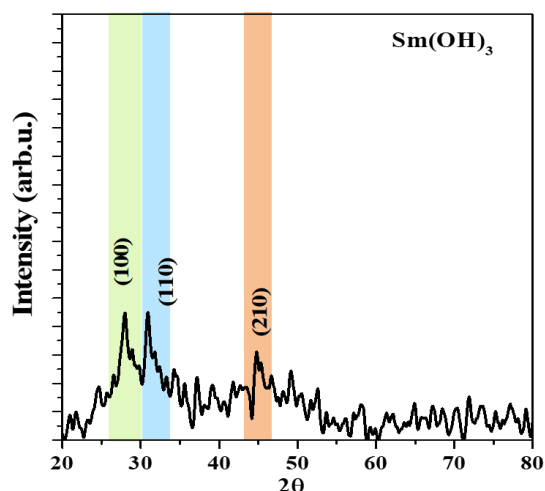
Table 2. Electron affinity and ionic radii of Sm^{3+} , Nd^{3+} , Ce^{3+} , and Ho^{3+} cations.

Cation	Electron affinity (kJ/mol)	Ionic radii (Å)
Sm^{3+}	109.1	1.08
Nd^{3+}	112.3	1.11
Ce^{3+}	115.5	1.15
Ho^{3+}	104.1	9.01

From the data compiled in Table 2, the semi-empirical correlation of electron affinity and ionic radii between Sm^{3+} , Nd^{3+} , Ce^{3+} and Ho^{3+} cations is evident [27]. Adding the chemical analysis of ∇H_{hyd}^0 to what was previously discussed, it is possible in principle to associate the correlation in crystal growth. We found in preliminary reports that the ions of rare earths, synthesized by CBD technique present the order of capture of OH^{-1} and CO_3^{2-} ions; $\text{Sm}(\text{OH})_3 > \text{NdOHCO}_3 > \text{CeO}_2 > \text{Ho}_2\text{O}_3$. According to the semi-empirical analysis, a certain correlation is observed in the capture of the competing ions, favoring the order proposed here for the creation of the final product. Is a plausible explanation for the crystal growth nanocrystalline compounds [7,8,14,17].

Preparation of samples

Details of experimental equipment for CBD technique, have already been reported by us [7,8,14,17]. The precursor reagents used were KOH (0.1 M), NH_4NO_3 (1.2 M), $\text{SC}(\text{NH}_2)_2$ (0.1 M). The water-soluble salts containing the Sm^{3+} , Nd^{3+} , Ce^{3+} , and Ho^{3+} cations at the corresponding molar concentration used are: $\text{Sm}(\text{NO}_3)_2 \cdot 5\text{H}_2\text{O}$ (0.2 M), $\text{Nd}(\text{NO}_3)_3 \cdot 5\text{H}_2\text{O}$ (0.3 M), $\text{Ce}(\text{NO}_3)_2 \cdot 5\text{H}_2\text{O}$ (0.2 M), and $\text{Ho}(\text{NO}_3)_3 \cdot 5\text{H}_2\text{O}$, respectively. Individually, the powders are prepared following the same crystal growth technique in each case reported by some of us in previous reports [7,8,14,17]. All reagents were of ~99.9% purity (Baker). The solutions are mixed in the aforementioned order in a 250 ml

**Figure 1.** XRD diffractogram of samarium hydroxide $\text{Sm}(\text{OH})_3$ nanocrystals.

beaker in different ratios, maintaining the proportions of the volumes, solution concentrations, pH (~8.2-8.5), stirring and temperature of ~20 °C were chosen, constants during the chemical synthesis. A precipitate-gel was obtained, which was filtered and washed several times with deionized water to remove ionic remnants. Crystalline structure characterization was carried out by X-ray diffraction (XRD) patterns registered in a Siemens D500 diffractometer, using the CuK_α line. Grain size (GS) was calculated using the Debye-Scherrer's formula: $\text{GS} = k\lambda/\beta\cos\theta$, where λ is the wavelength of X-ray radiation (~0.154 Å), k the Scherrer's constant ($k \sim 0.9$), θ (in radians) the characteristic X-ray radiation and β was the full-width-at-half-maximum (FWHM) of plane (in radians). Using the Williamson-Hall plot $\beta\cos\theta = k\lambda/\text{GS} + 4\epsilon\sin\theta$ equation, where ϵ is the strain, k a constant, β is the FWHM measured in radians and θ is the Bragg angle of the reflection, λ is the wavelength of X-ray used and ϵ is the strain of the crystallite.

Results and discussion

Figure 1 shows the X-ray Diffraction (XRD) diffractogram of samarium hydroxide $\text{Sm}(\text{OH})_3$. The inorganic nanomaterial is identified in the hexagonal crystalline phase (JCPDS 01-083-2036), which belongs to space group $P63/m$. Three crystalline angular reflections of small relative intensity are located at angular positions: $2\theta \sim 28.04^\circ$, $\sim 30.80^\circ$ and 47.0° , associated with (101), (210) and (210) crystal plane. Different crystalline planes of another material are not identified, which shows in principle that does not contain other than $\text{Sm}(\text{OH})_3$ nanocrystal. Experimental structural results are very close to those obtained by us; they were reported by Kang *et al.* [28]. The broadening of crystalline reflections, weak relative intensity, is generally associated with crystals with nanometric dimensions, as well as the presence of distributed amorphous regions that are found in a disorderly manner in different regions of the nanocrystals. Understanding, atomic, molecular and/or ionic disorder interactions is key to achieving control of materials at the molecular level, which is essential for various areas of physics and for nanotechnology [29]. This structural phenomenon molecular and/or ionic disorder created intrinsically in crystal growth. Self-organization of atoms and molecules into crystals plays a key role in diverse areas of science and the environment. On the other hand, the three -OH groups (-Sm-OH...OH-Sm-), generates weak short-range electrostatic interactions associated with van der Waals forces. However, weak in comparison to chemical bonds, their long-range nature and their collective effect play a strong role in the structure of molecules and their electrical interaction with surfaces [30]. A dislocation or Taylor's

Table 3. FWHM, GS and Dislocation density (δ) of $\text{Sm}(\text{OH})_3$ powders.

FWHM	Grain Size (nm)	Dislocation density, δ ($\times 10^{17}$ lines/m ²)
1.52	2.01	2.47
1.50	2.03	2.42
1.32	1.40	5.10

dislocation is a linear crystallographic defect or irregularity within a crystal structure that contains an abrupt change in the crystalline arrangement of ions or atoms [31]. Table 3 shows the full width at half-maximum (FWHM), GS and Dislocation density (δ) of $\text{Sm}(\text{OH})_3$ powders, the GS located at range ~ 1.4 - 2.03 nm.

Figure 2 show XRD of neodymium hydroxycarbonate NdOHCO_3 nanocrystals. The strong and sharp diffraction reflections indicate that the nanomaterial is well crystallized. The angular positions are located at $2\theta \sim 18.00^\circ, \sim 25.00^\circ, \sim 31.28^\circ, \sim 36.00^\circ, \sim 44.88^\circ, \sim 49.40^\circ, \sim 52.42^\circ, \sim 53.93^\circ, \sim 58.00^\circ, \sim 62.50^\circ, \sim 65.00^\circ, \sim 70.00^\circ,$ and $\sim 73.00^\circ$, corresponding to (002), (300) (300), (302), (004), (304), (134), (600). (602), (334), (306), (604), (630) and (362) crystal planes, respectively. Can be indexed to hexagonal structure NdOHCO_3 which are consistent with the data in the standard card (PDF 04-014-7918). Compared with the standard reflection, and those of (300), (302), (304), and (602) crystalline planes become strong. Thus, the changes in the relative intensity of the diffraction planes imply the orientation growth of NdOHCO_3 [32]. Also, reflections located at $2\theta \sim 43.27^\circ$, and $\sim 67.20^\circ$ can be seen (they are shown by an asterisk at the top of the crystal plane), which are identified as belonging to $\text{Nd}(\text{NO}_3)_3$ inorganic nanocrystal, a precursor reagent used in this work, not completely dissociated. A plausible explanation regarding the structural behavior of NdOHCO_3 , a first approximation is proposed: The chemical $-\text{OH}$ and CO_3^{2-} species in the nanocrystal, are located symmetrically surrounding Nd^{3+} cation, the electrostatic interaction in the crystal boundary creates van der Waals forces associated with hydrogen bonds. In addition, the electrostatic interaction created by $-\text{OH}$ and CO_3^{2-} ions located around the Nd^{3+} cation, generated by the electron cloud in the crystalline environment associated with the distribution of the electronic cloud of concentrated charge favors the creation of well-defined nanocrystals [33]. In the crystal growth carried out in our experimental conditions, strong and compact crystal-crystal

Table 4. FWHM, GS and Dislocation density (δ) of NdOHCO_3 nanocrystals.

FWHM	Grain size (nm)	Dislocation density, δ ($\times 10^{15}$ lines/m ²)
0.421	19.60	2.60
0.475	17.58	3.23
0.59	14.33	4.68
0.456	18.83	2.81
0.404	22.25	2.01

ordering is generated. The $-\text{Nd}-\text{O}-\text{H}\cdots\text{H}-\text{O}-\text{Nd}-$ chemical bonds, must be less favored with respect to the $-\text{Sm}-\text{OH}\cdots\text{HO}-\text{Sm}-$ bonds, therefore; crystal growth shows higher relative order. Table 4 shows FWHM, GS and Dislocation density (δ) of NdOHCO_3 nanocrystals, the GS located at range ~ 14.33 - 22.25 nm.

Figure 3 shows the XRD patterns of CeO_2 nanocrystal. Four broad crystalline reflections are observed, located at the following angular positions: $2\theta \sim 28.13^\circ, 32.75^\circ, 47.25^\circ$ and 56.35° . XRD patterns from $2\theta \sim 20$ - 80 range exhibit main crystalline plane, which are assigned to the (111), (200), (220) and (311) crystalline planes of CeO_2 . XRD pattern of CeO_2 shows broad reflections, which confirmed the formation of small-sized nanoparticles. The XRD results indicate that the CeO_2 nanocrystal, the patterns are in good agreement with a cubic structure (space group, $Fm\bar{3}m$ (No. 225 from bulk CeO_2)) (JCPDS Card No. 75-0076). In principle, it is possible to intuit the structural behavior associated with the phenomenon of electronic charge transfer from Ce^{4+} cation to the nearest neighbor according to $\text{Ce}^{4+} \rightarrow \text{Ce}^{3+} + e^-$. The $\text{O}^{2-}-\text{Ce}^{4+}$ charge transfer, we propose to attribute electronic intra-transitions on isolated Ce^{3+} ions in CeO_2 . The transfer of charge from one cation to another indexes the growth of nanocrystals favorably [34]. However, having been studied almost exclusively by chemists, molecular crystals still lack the appropriate investigations that reliably evaluate their reproducibility and some important drawbacks have diverted the interest of engineers from these crystals in science applications [35]. The structural phenomenon associated with load transfer correlates with the decrease in GS according to our

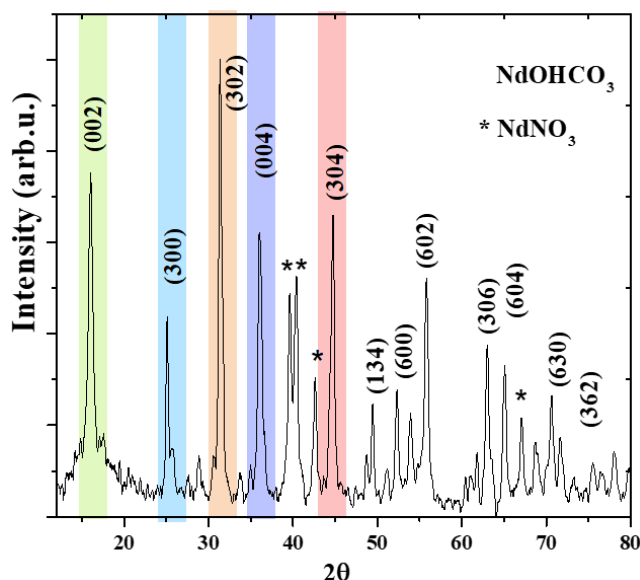


Figure 2. XRD of neodymium hydroxycarbonate NdOHCO_3 nanocrystals.

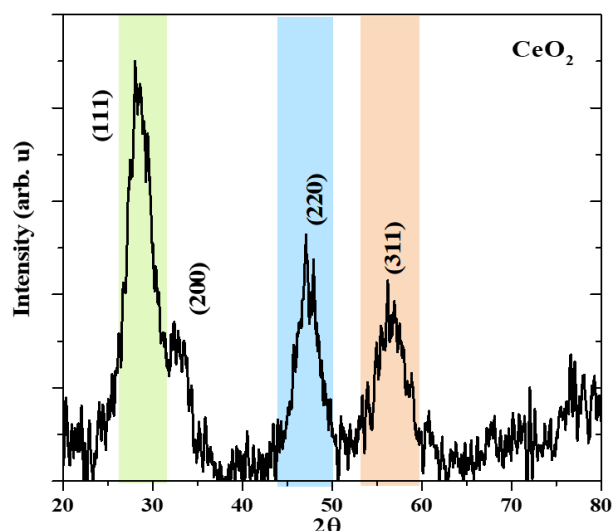


Figure 3. XRD of cerium oxide (CeO_2) nanocrystal.

Table 5. FWHM, GS and Dislocation density (δ) of CeO₂ powders.

FWHM	Grain Size (nm)	Dislocation density, δ ($\times 10^{17}$ lines/m ²)
2.96	2.28	1.93
2.78	3.05	1.07
2.64	2.60	1.47
3.08	2.25	1.97
3.66	1.65	3.67

preliminary report [34]. The crystalline structure is favored by creating nanocrystals and additionally amorphous regions are generated as a first approximation by disordered electrostatic interactions that have a short-range Ce=O...Ce=O, weaker than those presented by -Nd-OH...OH-Nd- and Sm.-OH...HO-Sm- interactions. Their conformation strongly depends on both the charge density and distribution along the sequence (i.e., charge decoration) as highlighted by recent experimental and theoretical studies that have introduced novel descriptors [36]. Table 5 shows FWHM, GS and Dislocation density (δ) of CeO₂ powders, the GS is located at range ~1.65-3.03 nm.

Figure 4 shows the diffractograms of X-Ray Diffraction (XRD) of Ho₂O₃ nanocrystals. The materials show crystalline reflections correspond to Ho₂O₃ in the cubic phase (00-067-0222 JCPDS). No reflections other than are observed. The diffraction planes located at $2\theta \sim 29.10^\circ$, $\sim 44.00^\circ$ and $\sim 53.20^\circ$ correspond to (222), (134) and (440) planes of Ho₂O₃ cubic phase, respectively [37]. Problems like polymorphic transitions, ions migration, slow crystallization and formation of crystalline aggregates stand out. Therefore, studies have focused on controlling the crystallization in order to determine the functionality of crystals. A plausible explanation of the crystalline and structural behavior is associated with the nucleation time, this generates that the small nanocoloids induce the formation of crystal small and prevent rapid growth to larger dimensions. The affecting chemical and physical parameters

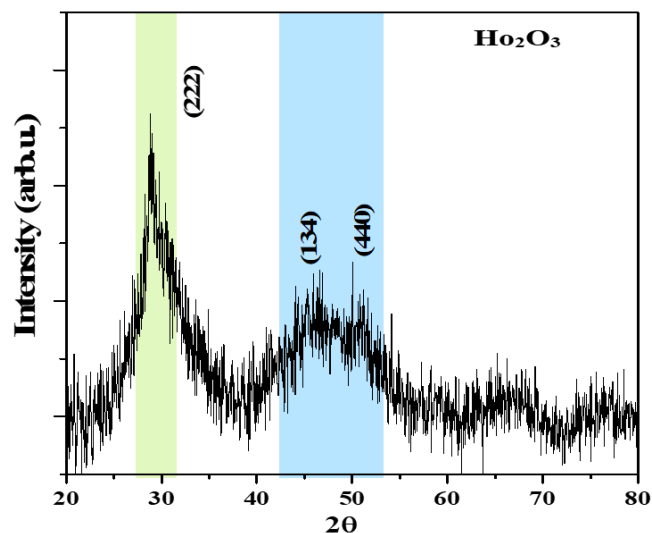


Figure 4. XRD of Holmium oxide Ho₂O₃ nanocrystals.

Table 6. FWHM, GS and Dislocation density (δ) of Ho₂O₃ powders.

FWHM	Grain Size (nm)	Dislocation density, δ ($\times 10^{16}$ lines/m ²)
1.52	6.08	2.70
1.50	3.72	7.22
1.32	5.64	3.14

factors (including nucleation temperature, freezing rate, and temperature fluctuation, etc.) on the size, number, distribution, and shape of crystals are also examined in detail [38]. The physicochemical phenomenon associated with crystal growth carried out systematically in aqueous solution, shows the importance of the parameters compiled in Tables 1 and 2, in which they are tentatively compared with each other semi-empirically. The approximate theoretical-experimental correlation with the chemical kinetic model examined here is observed. The kinetics of crystal growth is postulated semi-empirically with the change associated with the thermodynamic stability of the nanocrystal and the relative increase in GS, which presents the following order: Sm(OH)₃<Ho(OH)₃<CeO₂<NdOHCO₃ in the experimental conditions applied in the crystalline growth carried out in aqueous solution. Table 5 show FWHM, GS and Dislocation density (δ) of Ho₂O₃, the GS is located at range ~3.72-6.08 nm.

Using the Williamson-Hall (W-H) plot, defined by $\beta \cos \theta = k\lambda/GS + 4\epsilon \sin \theta$ equation, where ϵ is the strain, k a constant, β is the FWHM measured in radians and θ is the Bragg angle of the reflection, λ is the wavelength of X-ray used [21]. It can be determined from the slope (4ϵ) and from

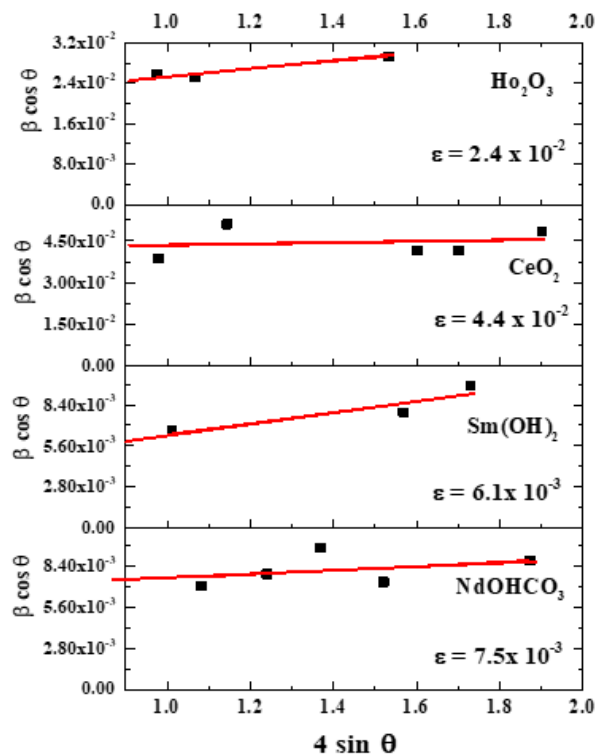


Figure 5. $\beta \cos \theta$ vs $4 \sin \theta$ plots for NdOHCO₃, Sm(OH)₃, CeO₂, and Ho₂O₃ nanocrystals.

the intercept ($k\lambda/GS$), respectively. The $\beta\cos$ vs $4\sin\theta$ plots for $\text{Sm}(\text{OH})_3$, NdOHCO_3 , CeO_2 and Ho_2O_3 nanocrystals powders are showed in Figure 5. The nearly flat W-H straight lines show that the nanomaterials possess less ε . The experimental results presented here do not exactly fit the linear behavior, which may be due to anisotropic variation in the residual ε . This disordered behavior is associated with the gradual incorporation ions and cation into the crystalline structure with a drastic change in the anisotropy, as was expected into the crystalline lattice. The ε is very much reduced in the smaller particles; a trend that is difficult to achieve in the processing of nanocrystals, and one can notice the smaller stress obtained in NdOHCO_3 and Ho_2O_3 samples. The anisotropy could be modified although the behavior will be for a deeper analysis to be done in due course.

Conclusions

The CBD technique is versatile, it presents physicochemical parameters of easy experimental control, and this allows us to semi-empirically compare the structural properties of the obtained nanocrystal. The chemical kinetics of crystal growth proposed in this report shows a certain approximate correlation with the physicochemical properties of the ions and/or cation examined here. However, the semi-empirical experimental results are not very far from each other when compared with the theoretical and the experimental part. According to the experimental results successfully obtained in this report, it is possible to obtain a semi-empirical correlation of the parameters associated with crystal growth: ionic radii, hydration enthalpy and electronic affinity of M^{3+} cation ($M^{3+} = \text{Sm}^{3+}$, Nd^{3+} , Ce^{3+} and Ho^{3+}), in principle they adjust to each other experimentally theoretical in an approximate way. The nanocrystals of these inorganic compounds grow with GS located at range ~ 1.04 - 22.25 nm, which is of interest to investigate the quantum confinement phenomenon, as well as for the application in the construction of optoelectronic devices. The Dislocation density (δ) shows that the nanocrystals present intrinsic crystalline defects (vacancies, interstices, stacking faults and grain boundaries), in semi-empirical correlation with the M^{3+} cation, these can be controlled experimentally.

Acknowledgements

We thank Centro de Investigación en Dispositivos semiconductores CIDS BUAP for the support provided for this research.

References

- [1]. A. Escudero, A.I. Becerro, C.C. Carrión, N.O. Núñez, M.V. Zyuzin, M. Laguna, D.G. Mancebo, M. Ocaña, W.J. Parak, *Nanophotonics* **6**, 881 (2017).
- [2]. M. Shafiq, I. Ahmad, S.J. Asadabadi, *J. Appl. Phys.* **116**, 103905 (2014).
- [3]. P.C. de S. Filho, J.F. Lima, O.A. Serra, *J. Braz. Chem. Soc.* **26**, 2471 (2015).
- [4]. N. Baig, I. Kammakam, W. Falath, *Mater. Adv.* **2**, 1821 (2021).
- [5]. Z. Gao, S. Rohani, J. Gong, J. Wang, *Engineering* **3**, 343 (2017).

- [6]. Z. Gao, X. Liu, C. Zhang, Y. Ren, *Cryst. Growth Des.* **22**, 2050 (2022).
- [7]. O. Portillo Moreno, R. Gutiérrez Pérez, R. Palomino Merino, M. Chávez Portillo, G. Hernández Téllez, E. Rubio Rosas, M. Zamora Tototzintle, *Optik* **148**, 142 (2017).
- [8]. O. Portillo Moreno, R. Gutiérrez Pérez, R. Palomino Merino, G. Hernández Téllez, M. Chávez Portillo, M.N. Márquez Especia, E. Rubio Rosas, H. Azucena Coyotécatl, *Optik* **130**, 1045 (2017).
- [9]. M. Powell, L.D. Sanjeeva, C.D. McMillen, K.A. Ross, C.L. Sarkis, J.W. Kolis, *Cryst. Growth Des.* **19**, 4920 (2019).
- [10]. I. Milisavljevic, Y. Wu, *BMC Mater.* **2**, 2 (2020).
- [11]. L. Spiridigliozzi, C. Ferone, R. Cioffi, M. Bortolotti, G. Dell'Agli, *Materials* **12**, 2062 (2019).
- [12]. P.Y.A. Guillén, O.V. Kharissova, R. Selvas, B.I. Kharisov, *Curr. Nanomater.* **4**, 39 (2019).
- [13]. K. Takagi, Y. Hirayama, S. Okada, W. Yamaguchi, K. Ozaki, *Sci. Technol. Adv. Mate.* **22**, 150 (2021).
- [14]. O. Portillo Moreno, R. Gutiérrez Pérez, R. Palomino Merino, M. Chávez Portillo, M.N. Márquez Especia, M. Hernández Hernández, S. Solis Saucedo, E. Rubio Rosas, *Optik* **135**, 70 (2017).
- [15]. M. Chávez Portillo, O. Portillo Moreno, E. Rubio Rosas, M. Zamora Tototzintle, R. Palomino Merino, G. Hernández Téllez, R. Gutiérrez Pérez, *Mater. Lett.* **151**, 134 (2015).
- [16]. O. Portillo Moreno, R. Gutiérrez Pérez, M. Chávez Portillo, M.E. Araiza García, G.E. Moreno, S. Cruz Cruz, E. Rubio Rosas, M. Hernández Lazcano, *Optik* **157**, 388 (2018).
- [17]. L. Serrano de la Rosa, M. Chávez Portillo, M.A. Mora-Ramírez, V. Carranza Téllez, M. Pacio Castillo, H. Juárez Santiesteban, A. Cortés Santiago, O. Portillo Moreno, *Optik* **216**, 164875 (2020).
- [18]. S.H. Anastasiadis, K. Chrissopoulou, E. Stratakis, P. Kavatzikidou, G. Kaklamani, A. Ranella, *Nanomater.* **12**, 552 (2022).
- [19]. R. Gutiérrez Pérez, O. Portillo Moreno, M. Chávez Portillo, L. Chaltel Lima, R. Agustín Serrano, E. Rubio Rosas, M. Zamora Tototzintle, *Mater. Lett.* **160**, 488 (2015).
- [20]. O. Portillo Moreno, R. Gutiérrez Pérez, R. Palomino Merino, H. Santiesteban Juárez, S. Tehuacanero Cuapa, E. Rubio Rosas, *Mater. Sci. in Semicon. Proces.* **72**, 22 (2017).
- [21]. R.P. Sharma, R. Bala, R. Sharma, U. Rychlewska, B. Warzajtis, *J. Fluor. Chem.* **126**, 967 (2005).
- [22]. P.R. Varadwaj, I. Cukrowski, H.M. Marques, *J. Phys. Chem. A* **112**, 10657 (2008).
- [23]. E. Brini, C.J. Fennell, M.F. Serra, B.H. Lee, M. Luksič, K.A. Dill, *Chem. Rev.* **117**, 12385 (2017).
- [24]. O. Portillo Moreno, O.R. Portillo Araiza, M. Chávez Portillo, V. Carranza Téllez, M.A. Vicencio Garrido, *Optik* **251**, 168470 (2022).
- [25]. M. Misin, M.V. Fedorov, D.S. Palmer, *J. Phys. Chem. B* **120**, 975 (2016).
- [26]. R.D. Shannon, *Acta Crystallogr. A* **32**, 751 (1976).
- [27]. J.M. Bijvoet, W.G. Burgers, G. Hägg, *Atomic (ionic) Radii and Building Principles. In: Early Papers on Diffraction of X-rays by Crystals*, Eds. J.M. Bijvoet, W.G. Burgers, G. Hägg (Springer, Boston, 1972).
- [28]. J.G. Kang, B.K. Min, Y. Sohn, *J. Mater. Sci.* **50**, 1958 (2015).
- [29]. F.L. Leite, C.C. Bueno, A.L.D. Róz, E.C. Ziemath, O.N. Oliveira Jr., *Int. J. Mol. Sci.* **13**, 12773 (2012).
- [30]. P.O. Bedolla, G. Feldbauer, M. Wolloch, S.J. Eder, N. Dörr, P. Mohn, J. Redinger, A. Vernes, *J. Phys. Chem. C* **118**, 17608 (2014).
- [31]. D. Hull, D.J. Bacon, *Introduction to dislocations*, 4th ed. (Butterworth-Heinemann, 2001).
- [32]. X. Shang, W. Lu, B. Yue, L. Zhang, J. Ni, Y. Iv, Y. Feng, *Cryst. Growth Des.* **9**, 1415 (2009).

- [33]. M.A. Boles, M. Engel, D.V. Talapin, [Chem. Rev. 116, 11220 \(2016\)](#).
- [34]. M. Chávez Portillo, O. Portillo Moreno, M.A. Mora-Ramírez, H. Juárez Santiesteban, C. Bueno Avendaño, Y. Panecatl Bernal, [Optik 248, 168178 \(2021\)](#).
- [35]. P. Naumov, D.P. Karothu, E. Ahmed, L. Catalano, P. Commins, J.M. Halabi, M.B.A. Handawi, L. Li, [J. Am. Chem. Soc. 142, 13256 \(2020\)](#).
- [36]. G. Bianchi, S. Longhi, R. Grandori, S. Brocca, [Int. J. Mol. Sci. 21, 6208 \(2020\)](#).
- [37]. Y. Fan, C. Miao, Y. Yue, W. Hua, Z. Gao, [Catalysts 11, 388 \(2021\)](#).
- [38]. M. Tan, J. Mei, J. Xie, [Crystals 11, 68 \(2021\)](#).

© 2023 by the authors; licensee SMCTSM, Mexico. This article is an open access article distributed under the terms and conditions of the Creative Commons Attribution license (<http://creativecommons.org/licenses/by/4.0/>).